Human Molecular Genetics, 2004, Vol. 13, No. 6 **641–650**
DOI: 10.1093/hmg/ddh061

On the molecular pathology of neurodegeneration in IMPDH1-based retinitis pigmentosa

Aileen Aherne[1,*], Avril Kennan[1], Paul F. Kenna[1,2], Niamh McNally[1], David G. Lloyd[3], Ian L. Alberts[3], Anna-Sophia Kiang[1], Marian M. Humphries[1], Carmen Ayuso[4], Paul C. Engel[5], Jing Jin Gu[6], Beverly S. Mitchell[6], G. Jane Farrar[1] and Pete Humphries[1]

[1]The Ocular Genetics Unit, Department of Genetics, Trinity College Dublin, Dublin 2, Ireland, [2]Research Foundation, Eye and Ear Hospital, Dublin 2, Ireland, [3]De Novo Pharmaceuticals, Compass House, Vision Park Histon, Cambridge CB4 9ZR, UK, [4]Fundacion Jimenez Diaz, Clinica de Nuestra Senora de la Conception, Avda de los Reyes Catolicos 2 (Ciudad Universitaria), 28040 Madrid, Spain, [5]Department of Biochemistry and Conway Institute of Biomolecular and Biomedical Research, University College Dublin, Belfield, Dublin 4, Ireland and [6]Lineberger Comprehensive Cancer Center, Department of Pharmacology, University of North Carolina at Chapel Hill, NC 27599, USA

Received November 7, 2003; Revised and Accepted January 12, 2004

Retinitis pigmentosa (RP), the hereditary degenerative disease of the photoreceptor neurons of the retina, probably represents the most prevalent cause of registered blindness amongst those of working age in developed countries. Mutations within the gene encoding inosine monophosphate dehydrogenase 1 (*IMPDH1*), the widely expressed rate-limiting enzyme of the *de novo* pathway of guanine nucleotide biosynthesis, have recently been shown to cause the RP10 form of autosomal dominant RP. We examined the expression of IMPDH1, IMPDH2 and HPRT transcripts, encoding enzymes of the *de novo* and salvage pathways of guanine nucleotide biosynthesis, respectively, in retinal sections of mice, the data indicating that the bulk of GTP within photoreceptors is generated by IMPDH1. *Impdh1*$^{-/-}$ null mice are shown here to display a slowly progressive form of retinal degeneration in which visual transduction, analysed by electroretinographic wave functions, becomes gradually compromised, although at 12 months of age most photoreceptors remain structurally intact. In contrast, the human form of RP caused by mutations within the IMPDH1 gene is a severe autosomal dominant degenerative retinopathy in those families that have been examined to date. Expression of mutant IMPDH1 proteins in bacterial and mammalian cells, together with computational simulations, indicate that protein misfolding and aggregation, rather than reduced IMPDH1 enzyme activity, is the likely cause of the severe phenotype experienced by human subjects. Taken together, these findings suggest that RP10 may represent an attractive target for therapeutic intervention, based upon a strategy combining simultaneous suppression of transcripts from normal and mutant IMPDH1 alleles with supplementation of GTP within retinal tissues.

INTRODUCTION

Retinitis pigmentosa (RP), an hereditary degenerative disease of the photoreceptor neurons of the retina, represents the most prevalent cause of registered visual handicap among those of working age in developed countries (1,2). Disease pathology primarily affects rod photoreceptor cells, which gradually die, precipitating symptoms of nyctalopia (night blindness). Without the support of rods, cone photoreceptors also begin to degenerate, usually resulting in a severe narrowing of the visual fields and eventually complete blindness. RP, or syndromes incorporating the disease, is transmitted according to autosomal dominant, recessive, X-linked recessive, digenic or mitochondrial modes of inheritance and occasional pedigrees have been encountered displaying so-called digenic–diallelic or digenic–triallelic hereditary patterns (3). The disease is immensely heterogeneous at the genetic level, 29 genes having so far been implicated in disease pathology, rendering RP, without doubt, one of the most functionally complex of Mendelian hereditary diseases (4) (RetNet database; www.sph.uth.tmc.edu/Retnet/).

*To whom correspondence should be addressed. Tel: +353 16082484; Fax: +353 16083848; Email: aaherne@tcd.ie

One of the most interesting recent observations to have emerged from studies of the molecular genetics of RP, or syndromes incorporating the disease, is that a number of genes encoding transcripts or proteins that are expressed in many tissues of the body have been shown to cause a disease pathology only or primarily in the retina. Included are the mitochondrial *MTTS2* gene (5), genes encoding three pre-mRNA splicing factors (6–8) and inosine monophosphate dehydrogenase type 1 (*IMPDH1*) (9,10). Mutations within the IMPDH1 gene cause the RP10 form of autosomal dominant RP, those families identified to date exhibiting an early onset, severe retinal degeneration (9–11).

IMPDH1 functions as a tetramer composed of four identical subunits, each of 55 kDa, and is the rate-limiting enzyme of the *de novo* pathway of guanine nucleotide biosynthesis. It converts inosine monophosphate into xanthosine monophosphate, which is then converted into guanosine diphosphate (GDP) and triphosphate (GTP). The functionally related enzyme, IMPDH2, performs a similar role, the two proteins sharing 84% identity at the amino acid level (12). Guanine nucleotides may also be synthesized in the so-called salvage pathway by the enzyme hypoxanthine phosphoribosyl transferase (HPRT). Both IMPDH isoforms exhibit widespread expression patterns but their regulation and levels of expression differ considerably (13). Expression of IMPDH1 has previously been shown to be tissue-specific, with high levels of expression for example in the lung, thymus and brain, but barely detectable levels of expression in liver and testis (14). In mice, loss of both alleles of the *Impdh* type 2 gene results in very early embryonic lethality (15). A mouse deficient in the *Impdh* type 1 gene has recently been generated using standard gene targeting techniques (14). In contrast to the *Impdh2* knockout it was found that Impdh type I enzymatic activity is not essential for normal mouse development or fertility.

We have now explored the patterns of expression of *Impdh1*, *Impdh2* and *Hprt* genes within the murine retina, showing that *Impdh1* transcripts are in relatively high abundance in photoreceptors in comparison to those from the *Impdh2* and *Hprt* genes, and it is therefore highly likely that IMPDH1 is responsible for the bulk of GTP supply to the photoreceptor cells. We also show that disruption of the *Impdh1* gene induces a mild retinopathy in mice. In addition, the functions and properties of wild-type and mutant human IMPDH1 proteins have been explored by expression studies in *E. coli* and mammalian Hek293T cells and by computational simulation studies. Together these data suggest that the severe symptoms of RP10 could be substantially ameliorated by simultaneous ablation of normal and mutant *IMPDH1* transcripts within photoreceptor neurons, rendering this form of retinal degeneration a highly attractive therapeutic target using current suppression technologies.

RESULTS

Impdh and *Hprt* expression in the murine retina

In order to assess expression patterns of IMPDH1, IMPDH2 and HPRT in retinal tissues, *in situ* hybridizations were carried out using *riboprobes* specific for transcripts derived from these genes on mouse retinal cryosections. EST data obtained for the *IMPDH2* gene (UniGene database; www.ncbi.nlm.nih.gov/entrez/query.fcgi?db = unigene) indicate that this isoenzyme is expressed in retinal pigment epithelium (RPE) libraries, hence *Impdh2 in situ* hybridizations were performed on retinal sections from CD1 mice, which do not possess pigment in the RPE. The results of this analysis indicate that *Impdh1* is preferentially and strongly expressed within photoreceptor cells (Fig. 1A). Conversely, little or no *Impdh2* expression is detectable in photoreceptors and only low levels of *Hprt* transcript are observed (Fig. 1B and C). These results thus indicate that IMPDH1 is largely responsible for the production of guanine nucleotides within photoreceptor cells. In mice lacking the *Impdh1* gene, it has previously been reported that there is no elevation in expression levels of *Impdh* type 2 or *Hprt* transcripts detectable in response to a deficiency of *Impdh* type 1, in a number of tissues examined (14). It is very likely, therefore, that in the case of a defective or absent IMPDH1 protein in the retina, IMPDH2 and HPRT may not be able to substitute for the loss of IMPDH1 activity. This is particularly relevant given that the retina is one of the most energy-demanding tissues of the body and that photoreceptor cells have a high requirement for GTP within the visual transduction cycle (16).

Retinal structure and function in *Impdh1*$^{-/-}$ mice

A rational interpretation of the above data is that IMPDH1 is important to normal photoreceptor function. Hence, we evaluated photoreceptor activity in the retinas of *Impdh1*$^{-/-}$ mice using electroretinography (ERG). Rod-isolated responses (Fig. 2A), light-adapted cone responses to single flash (Fig. 2B) and maximal, dark-adapted, combined rod and cone responses (Fig. 2C) were recorded at 6 weeks of age and 5, 8, 11 and 13 months. At 11 months of age all responses showed a significant reduction in a- and b-wave amplitudes (Fig. 2A–C) and, in the case of the cone responses, significant delay in b-wave timing (Fig. 2B). Further deterioration was noted by 13 months. In the case of the maximal, dark-adapted, combined rod and cone responses, progressive reduction in wave amplitudes was noted from 5 months of age, indicating disturbance of phototransduction. This may be explained by disturbance in cGMP-dependent cation channel function, which requires a constant turnover of cGMP, which must be synthesized from GTP. A reduction in ERG amplitude, brought about by membrane hyperpolarization and closing of these channels, may be due to the disturbance in guanine biosynthesis consequent to lack of IMPDH1 activity.

It is notable that the electroretinographic disturbances observed in *Impdh1*$^{-/-}$ mice appear to be much milder than those recorded in humans with dominant *IMPDH1* mutations, where generally all ERG responses are unrecordable by the end of the second decade. The response in an affected 17-year-old male from a large RP10 family (9,11) to the maximal intensity flash presented in the dark-adapted state, which normally elicits a mixed rod–cone response, indicates that there is no recordable photoreceptor activity (Fig. 2D). The *Impdh1*$^{-/-}$ mouse model at 4 months of age, which we estimate to be approximately equivalent to a teenage human subject in terms of relative lifespan, displays no detectable structural or functional degeneration of the retina. In addition, photoreceptor

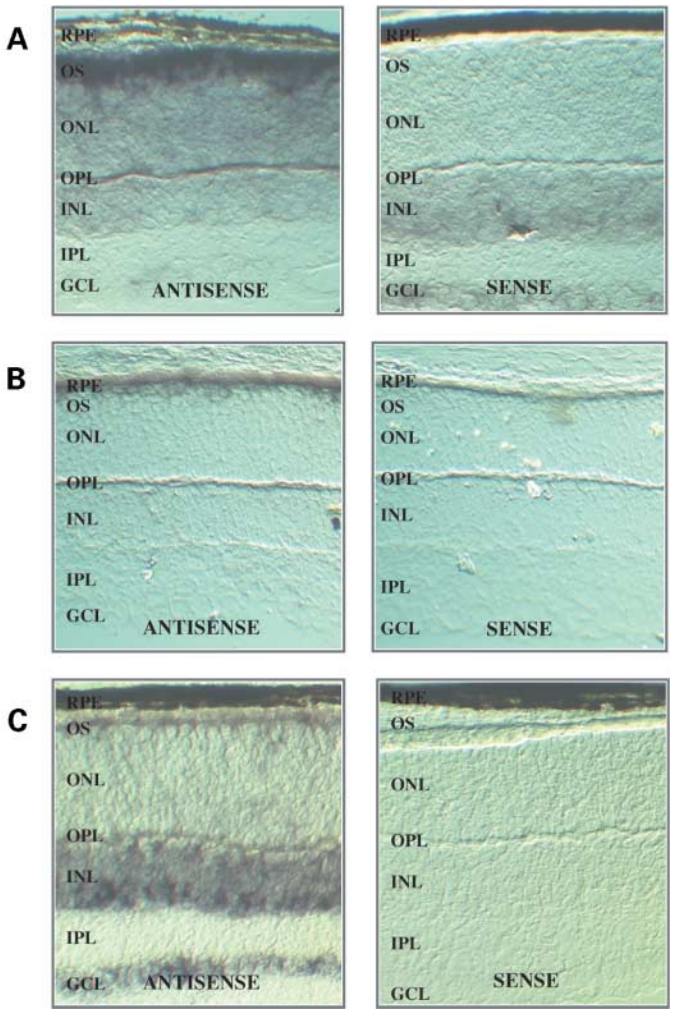

Figure 1. *In situ* hybridization studies on mouse retinal cryosections. Retinal sections with antisense and sense DIG-labelled riboprobes for (**A**) *Impdh1*, (**B**) *Impdh2* and (**C**) *Hprt* are shown. The *Impdh2 in situs* are performed on CD1 mouse retinas, which lack the pigment normally found in the RPE, while the *Impdh1* and *Hprt in situs* are performed on wild-type pigmented retinas. Strong expression of *Impdh1* is detected in the photoreceptor neurons. *Impdh2* expression appears to be restricted to the RPE, with possibly very low level staining in the photoreceptor outer segments. Analysis of *Hprt* reveals expression in the inner nuclear and ganglion cell layers along with a lower level of expression in the photoreceptors. (RPE) retinal pigment epithelium, (OS) outer segments, (ONL) outer nuclear layer, (OPL) outer plexiform layer, (INL) inner nuclear layer, (IPL) inner plexiform layer, (GCL) ganglion cell layer. 200× magnification.

dysfunction in the *Impdh1*$^{-/-}$ mouse is not the result of loss of photoreceptor cell viability, since the outer nuclear layer thickness of the retinas in these mice is similar to wild-type retinas up to 10 months of age (Fig. 3A–C), and even by 13 months of age there is only marginal loss of nuclei from the outer nuclear layer of the retina (data not shown). Preliminary evidence suggests some degree of disorganization of photoreceptor outer segments in older animals which is akin to a mild RP-like retinopathy. Thus, IMPDH1 does not appear to be essential for normal retinal development or early visual function. In the light of such observations, it appears unlikely that the autosomal dominant segregation pattern which is characteristic of the RP10 form of retinitis pigmentosa, is caused as a result of 'haploinsufficiency' for the normal *IMPDH1* gene product. Rather, disease pathology is probably caused by a dominant-negative phenotypic effect exerted by mutant protein.

Functional analysis and mammalian expression of wild-type and mutant IMPDH1 proteins

Two amino acid substitutions, Arg224Pro and Asp226Asn, originally identified in RP10 families (9,10), lie in the second CBS domain that forms part of a smaller flanking subdomain of the IMPDH enzyme (17). This region lies adjacent to the catalytic domain and is not thought to be required for activity (18,19). In order to assess possible effects of these two established IMPDH1 mutations on the functional activity of the expressed enzyme, the wild-type and two mutant human *IMPDH1* proteins were expressed in a bacterial expression system with incorporation of a His-tag for purification purposes. Protein fractions were purified from soluble cell lysates and enzymatic activity was determined by measuring the absorbance increase caused by reduction of NAD^+ (20). Specific enzyme activities for wild-type, Arg224Pro and Asp226Asn IMPDH1 enzymes were averaged at 1.22, 1.30 and 1.28 $\mu mol\,min^{-1}\,mg^{-1}$, respectively. Enzyme activities were measured on soluble protein only and all three enzymes showed similar levels of activity for up to 7 days. Therefore, no significant differences in specific enzyme activity were detectable between the wild-type and mutant IMPDH1 proteins. Calculated activities were also comparable to previously published reports of IMPDH1 specific enzyme activity levels (21). A dramatic reduction in enzyme activity would be expected if the disease-causing effects of the mutations were primarily attributable to diminished activity under physiological conditions.

Mutant IMPDH1 proteins were found to exhibit marked decreased solubility in comparison to wild-type when expressed at a temperature of 37°C in bacterial cells (data not shown). In order to investigate this observation further, human embryonic kidney (HEK) 293T cells were transfected with mammalian expression constructs containing wild-type, Arg224Pro or Asp226Asn mutant *IMPDH1* sequences, with incorporation of a His-tag for protein detection purposes. After harvesting, cells were separated into total cell protein, soluble cytosolic, nuclear and insoluble pelleted fractions, which were subsequently analysed by SDS–PAGE electrophoresis (Fig. 4A) and western blotting (Fig. 4B). Wild-type and mutant IMPDH1 proteins were expressed at similarly high levels in whole cell extracts with a band clearly visible at 55 kDa (Fig. 4A). No protein band of this size was evident in cells transfected with a construct that did not contain an *IMPDH1* cDNA insert. Following analysis of cellular fractions obtained after further purification steps, wild-type IMPDH1 protein was shown to localize in the soluble cytosolic fraction, while no mutant protein was detectable in this fraction. Both mutant proteins exhibited considerably decreased solubility and as a result almost all of the mutant protein localized in the final pellet, which was re-suspendable in strong denaturant. Accordingly, we hypothesize that such mutant IMPDH1 proteins may be

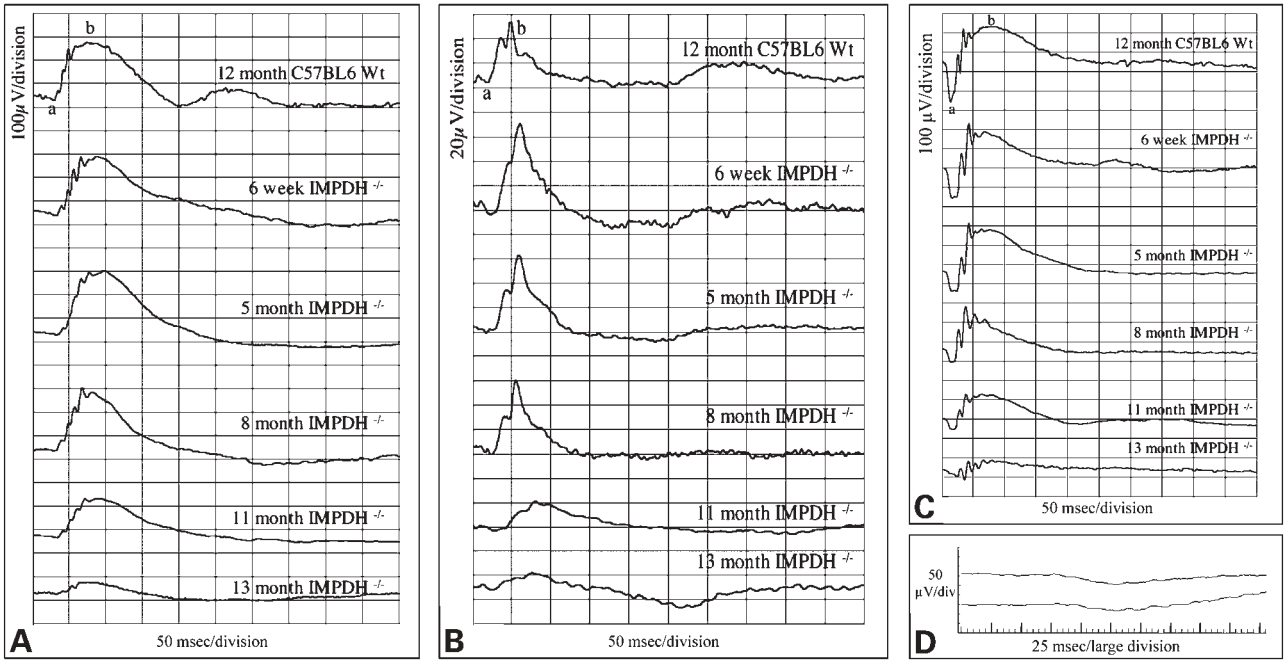

Figure 2. ERG analysis in *Impdh1*$^{-/-}$ mice. (**A**) Rod-isolated responses, (**B**) light-adapted cone responses to single flash and (**C**) maximal, dark-adapted, combined rod and cone responses were recorded in a 12-month C57 wild-type animal, and *Impdh1*$^{-/-}$ animals at 6 weeks of age, 5 months, 8 months, 11 months and 13 months. At 11 months of age all responses showed a significant reduction in a- and b-wave amplitudes and, in the case of the cone responses, significant delay in b-wave timing. Further deterioration was noted by 13 months. In the case of the maximal, dark-adapted, combined rod and cone responses progressive reduction in a-wave amplitude was noted from 5 months of age indicating disturbance of phototransduction. (**D**) ERG analysis of combined rod and cone response in a 17-year-old affected patient harbouring an Arg224Pro IMPDH1 mutation shows completely diminished responses.

mis-folded, resulting in the formation of insoluble aggregates within the cell cytosol.

Computer protein modelling studies on mutant IMPDH1

To further investigate the existence of possible tertiary structural perturbation in mutant IMPDH1, we undertook a series of molecular modelling computational simulations for the Arg224Pro mutation. Proline residues located within α-helices have a tendency to distort the standard helical arrangement by causing the structure to kink about the position of the proline residue (22). To test the hypothesis that a mutation from Arg to Pro could result in a mutant protein with perturbed structure correlating to impaired *in vitro* and *in vivo* function, structural homology models were constructed from both Arg-wild-type and Pro-mutant IMPDH1 sequences, building from available crystal structures of human (17) and non-human (*Cricetulus griseus*) (18) IMPDH which exhibited high homology to our sequences of interest. The resultant wild-type and mutant structures were subjected to an extensive computational molecular dynamics simulation to challenge and refine the models (23). We observed no significant deviation in structure for the wild-type protein post-dynamics (data not shown), but significant structural perturbation was noted in the mutant structure around the area of point mutation (Arg224 to Pro224) by the end of the simulation run. Figure 5 illustrates the end-point results from molecular dynamics simulation on mutant (pink) and wild-type (blue) IMPDH1 homology models. The Arg to Pro mutation in the 'bud' or flanking region is highlighted in green in both models. The perturbation of predicted tertiary structure is clearly visible as the mutated protein loses cohesion of structure in the 'bud' domain, distant from the principal catalytic domain. Such structural perturbation would undoubtedly disrupt the formation of the biological homotetramer subunit and correlates to the observed physical and functional data for the mutant protein.

DISCUSSION

The RP10 gene was initially localized on chromosome 7q as a result of a systematic genetic linkage study mounted on DNA from a large Spanish family (11). It is estimated, based on the number of pedigrees so far identified with the RP10 form of retinopathy, that this genetic sub-type of disease accounts for 3–5% of autosomal dominant cases of RP (24). The *in situ* hybridization data presented here clearly demonstrate high levels of *Impdh1* expression within the photoreceptor cell layer of mouse retinas, in comparison to levels of transcript derived from the *Impdh2* and *Hprt* genes. The retina has the highest metabolic rate of any tissue of the body, photoreceptors having a particularly high requirement for GTP in visual transduction processes (16). Therefore, we suggest that depletion of the GTP pool over time is the most likely explanation for the reduction in ERG amplitudes seen in the retinas of older *Impdh1*$^{-/-}$ mice and is the cause of the mild retinopathy that such animals develop. In addition, the human and mouse IMPDH1 sequences share 98% identity at the protein level which strongly

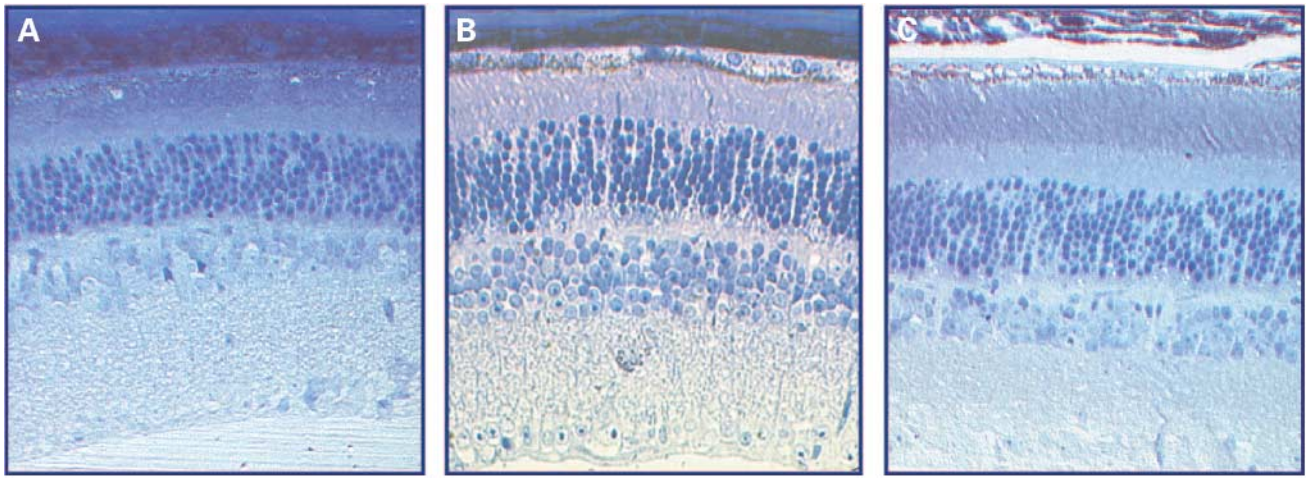

Figure 3. Light micrographs of retinal sections from *Impdh1*$^{-/-}$ mice. Sections shown are (**A**) 6-month *Impdh1*$^{-/-}$, (**B**) 10-month *Impdh1*$^{-/-}$, (**C**) 10-month wild-type C57/BL6. The outer nuclear layer thickness of *Impdh1*$^{-/-}$ retina is virtually indistinguishable from that of wild-type up to 10 months of age.

suggests that IMPDH1 function in the retina is highly conserved amongst species.

The *Impdh1*$^{-/-}$ mouse represents the first reported model carrying a targeted deletion of a ubiquitously expressed dominant RP-associated gene and has been shown to display no detectable structural or functional degeneration of the retina up to 5 months of age. In contrast, previously reported murine models in which there is a targeted deletion of a dominant RP-associated gene, including the *rhodopsin*, *rds-peripherin*, *Rp1* and *Crx* knockout mouse models, have resulted in phenotypes in which there is significant degeneration of photoreceptor cells and in many cases, completely diminished ERG amplitudes by 5 months of age (25–28). While it will not be possible to directly compare the molecular pathologies associated with autosomal dominant and recessive (represented by the *Impdh1*$^{-/-}$ null mouse) forms of IMPDH1-based disease, unless human subjects with the latter form of disease are identified, the data presented nevertheless strongly support the concept that the retinopathy in human subjects is very much more severe than the disease state which has been shown to occur as a result of a targeted disruption of the *Impdh1* gene in mice.

The studies presented on mutant IMPDH1 proteins show that there are no detectable differences in enzyme activity when compared with wild-type, but that a substantial difference in solubility between wild-type and mutant proteins is observable in both bacterial and mammalian cells. Such observations, along with distinct perturbations in protein structure predicted by computer modelling of mutant IMPDH1 structure, point to a probable dominant-negative molecular pathology for RP10, as a result of alterations in the folding and solubility of the mutant protein. It is of note that similar differences in solubility between wild-type and mutant proteins have been demonstrated in relation to the RP-associated splicing factor PRPF31 (29), and protein folding defects associated with rhodopsin mutations that lead to aggresome formation have also been described (30–32). Hence, in RP10, mutant IMPDH1 protein misfolding and subsequent aggregation may be a central event in the initiation of neuronal cell death, as it is in a range of other hereditary or multifactorial neurodegenerative diseases including Alzheimer disease, Parkinson disease and amyotrophic lateral sclerosis (33–35).

Notwithstanding recent successes in restoration of visual function or preservation of the retina in autosomal recessive forms of degenerative retinopathy, including the Briard dog model of Leber congential amaurosis (36) and the RCS rat following AAV-mediated delivery of therapeutic genes to retinal tissues (37), the extensive intragenic heterogeneity associated with autosomal dominant forms of retinal degeneration is a major impediment to the development of successful and economically viable therapeutics. For example, in excess of 200 different mutations have been encountered within the rhodopsin and RDS-peripherin genes alone (Retina International Database; www.retina-international.org/sci-news/rhomut.htm). While the *IMPDH1* gene was implicated in disease etiology only within the last 2 years, the number of mutations identified within the gene in patients with RP is already rising (38). Hence suppression strategies targeting individual mutations are unlikely to be viable in economic terms. While a series of so-called mutation-independent suppression-replacement strategies has been described, such approaches involve two major steps, the simultaneous suppression of transcripts derived from both normal and mutant alleles, together with the introduction of a replacement gene, altered, for example at third-base degenerate sites, such as to escape suppression but nevertheless encoding functional protein (39–41). Insights we have gained into the nature of the molecular pathology of retinal degeneration in RP10, combined with studies on the autosomal recessive form of disease in the *Impdh1*$^{-/-}$ mouse, suggest that RP10 may be a particularly attractive potential therapeutic target for two reasons. Firstly, only a single suppression step, involving simultaneous silencing of both normal and mutant alleles of the *IMPDH1* gene would, in principle, be sufficient to remove the major dominant negative pathological effect of mutant IMPDH1 protein, leaving a situation in which photoreceptor neurons continue to survive and remain sufficiently functional such as to provide useful vision, possibly well into adult life. Secondly, while gene silencing using RNA interference is now an established

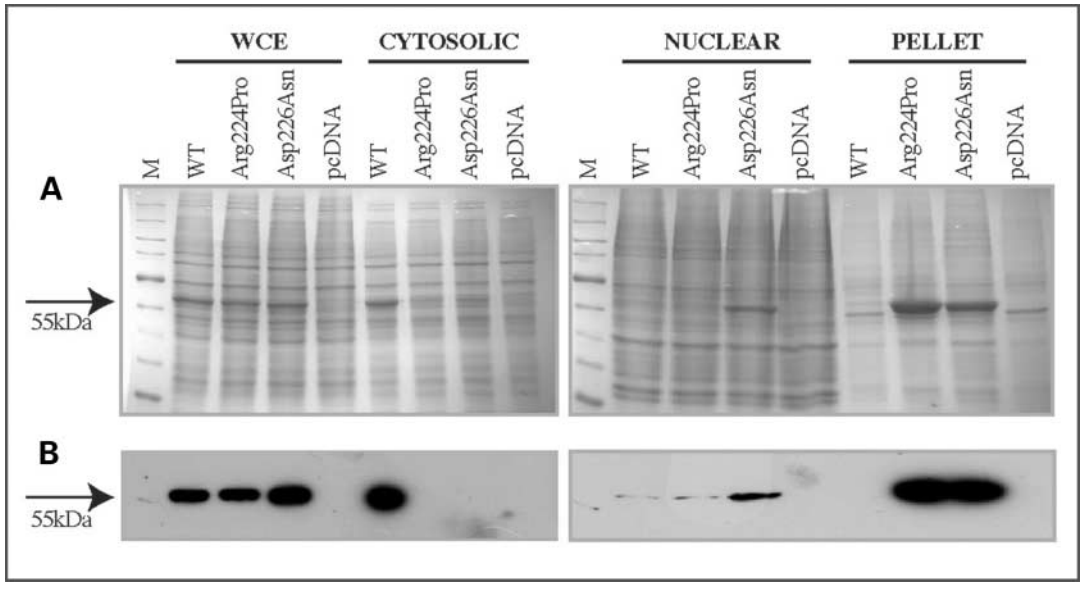

Figure 4. Analysis of wild-type and mutant IMPDH1 proteins expressed in HEK293T cells. (**A**) SDS–PAGE with Coomassie blue staining of protein extracts from cells transfected with pcDNA3.1/His constructs containing wild-type (WT), Arg224Pro and Asp226Asn mutant IMPDH1 sequences, and pcDNA vector alone (negative control). Transfected cells were separated into whole cell extracts (WCE), soluble cytosolic fraction, nuclear fraction and final pelleted fraction. M = Molecular mass marker. (**B**) Western blot of an identical gel with protein transfer onto nitrocellulose membrane and probed with Anti-His antibody and HRP-conjugated secondary antibody. M = 50 kDa His-tag protein (positive control).

technique in mammalian systems (42), discrimination between normal and mutant transcripts at the level of single nucleotides has so far met with only partial success (43). In the case of the therapeutic approach outlined here, such constraints do not apply, since there is not a requirement to target single base changes.

In order to provide a rationale for clinical investigation of this form of therapeutic approach in human subjects, confirmation of minimal disease pathology in larger animals, ideally primates, following ablation of IMPDH1 transcripts in retinal tissues will be required. It will also be of interest to explore whether delivery to ocular tissues of XMP or GTP (using, for example, the technique of iontophoresis) might provide sufficient supplementation of these compounds such as to fully restore function in remaining photoreceptors of the *Impdh1*$^{-/-}$ mouse.

MATERIALS AND METHODS

In situ hybridizations

In situ hybridizations involved the use of digoxigenin (DIG)-labelled riboprobes on frozen cryosections. Sense and antisense DIG-labelled probes were generated from PCR templates which had incorporated T7 and T3 promoters. Sections were fixed in paraformaldehyde post cutting, treated with active DEPC and hybridisation with both sense and antisense probes was allowed to proceed overnight at 58°C. Following stringent washes with SSC, incubation with an AP coupled, anti-DIG antibody was carried out. Binding of the probes was detected using NBT/BCIP solution. Sections were mounted and analysed using a Zeiss Axioplan 2 microscope.

Mouse electroretinography

Mouse ERGs were recorded at 6 weeks of age (two animals), 5 months (six animals), 8 months (four animals), 11 months (five animals) and 13 months (three animals). Animals were dark-adapted overnight and prepared for electroretinography under dim red light. Pupillary dilatation was achieved by instillation of cyclopentalate 1% and phenylephrine HCl 10%. The subjects were anaesthetized by means of ketamine (2.08 mg per 15 g body weight) and xylazine (0.21 mg per 15 g body weight) injected intraperitoneally. Standardized flashes of light were presented to the mouse in a Ganzfeld bowl to ensure uniform retinal illumination. The ERG responses were recorded simultaneously from both eyes by means of contact lens electrodes (Medical Workshop, Groningin, Netherlands) using amethocaine 1% as topical anaesthesia and Vidisic (Dr Mann Pharma, Germany) as a conducting agent and to maintain corneal hydration. A reference electrode was positioned subcutaneously approximately 1 mm from the temporal canthus and the ground electrode placed subcutaneously anterior to the tail. The responses were analysed using RetiScan RetiPort electrophysiology equipment (Roland Consulting Gmbh). The protocol used was based on that approved by the International Clinical Standards Committee for human electroretinography. Rod-isolated responses were recorded using a dim white flash (−25 dB maximal intensity) presented in the dark-adapted state. The maximal combined rod–cone response to the maximal intensity flash was then recorded. Following light adaptation for 10 min to a background illumination of 30 candelas per m^2 presented in Ganzfeld bowl the cone-isolated responses were recorded to the maximal intensity flash (3 candelas per m^2 per second) presented as a single flash and 10 Hz flickers. a-Waves were measured from the baseline to the

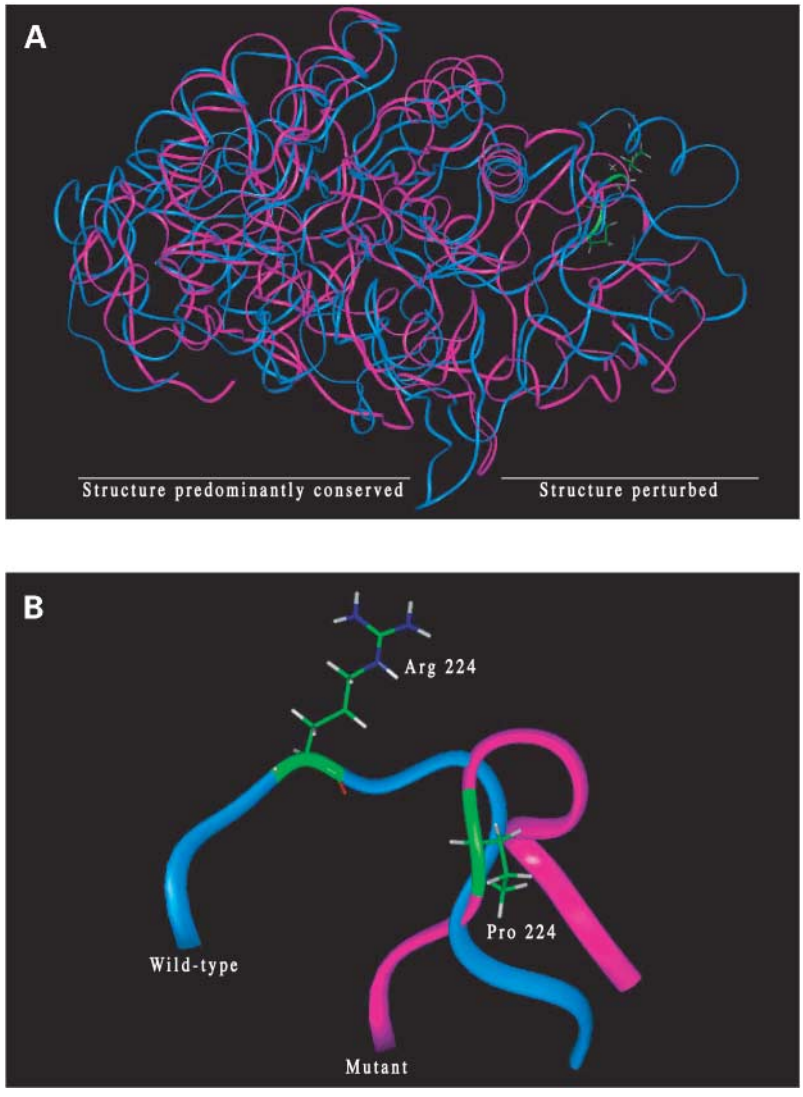

Figure 5. Computer modelling of wild-type and mutant IMPDH1 proteins. (**A**) Endpoint comparison of molecular dynamics simulation run solutions for wild-type (blue) and mutant (pink) homology models of human IMPDH1. (**B**) Model of IMPDH1 mutant product (pink) exhibits significant predicted structural perturbation in region of Arg to Pro point mutation when compared to model of wild-type protein (blue). The Arg to Pro mutation in the 'bud' or flanking region is highlighted in green in both models.

trough and b-waves from the baseline (in the case of rod-isolated responses) or from the a-wave trough.

Retinal histology

Eyes were perfused overnight with a mixture of 2.5% glutaraldehyde and 2% paraformaldehyde in 0.1 M phosphate buffer, pH 7.4, and processed in Epon. Sections 1 μm thick were cut through the optic nerve head, along the vertical meridian of the eye, and were stained with toludine blue for light microscopy.

Expression of wild-type and mutant His-tagged IMPDH1 in *E. coli*

Primers were designed to introduce *Xho*I sites at either end of the wild-type *IMPDH1* cDNA sequence in the pGEM vector (21). The 1.5 kb cDNA was amplified by PCR with *Pfu* DNA polymerase (Stratagene). *IMPDH1* cDNA inserts were then cloned into the *Xho*I site of the pET-15b vector (Novagen), which incorporates a His-tag at the N-terminus of the protein sequence. The single point mutations CGC to CCC (Arg224Pro) and GAC to AAC (Asp226Asn) were introduced using the Quikchange site-directed mutagenesis kit (Stratagene). All inserts were sequenced completely using automated sequencing on an ABI 310 Genetic Analyzer (Perkin Elmer, Shelton, CT, USA) and Big Dye Terminator chemistries (Perkin Elmer), to verify the presence of intended mutations and the absence of further unwanted mutations. Constructs were transformed into *E. coli* BL-21(DE3) for protein expression. Cells were grown at 37°C in 100 ml LB to an OD_{600} of 1.0 and induced with 400 μM IPTG. Induction of protein expression was carried out at 25°C because at higher temperatures only very low levels of IMPDH1 protein,

especially mutant protein, were detectable in soluble cell lysates. A lower induction temperature improves protein solubility and helps prevent inclusion-body formation. Cells were harvested 3–5 h post-induction, resuspended in Ni-NTA bind buffer (Novagen), treated with lysozyme and sonicated. Soluble cell lysates were enriched for His-tagged protein using Ni-NTA His-bind resin (Novagen) according to manufacturers' instructions, and relatively pure samples of IMPDH1 protein were isolated. Proteins samples were run on 10% SDS–polyacrylamide gels and stained with Coomassie Blue.

Enzyme activity assay of recombinant IMPDH1 proteins

Protein concentration was determined using the Bio-Rad protein assay and bovine IgG as standard. The standard enzyme assay buffer contained 0.1 M Tris, 0.1 M KCl, 3 mM EDTA, 2 mM DTT pH 8.0, and the substrates 400 μM IMP and 400 μM nicotinamide adenine dinucleotide (NAD). The reaction was started by addition of 5–25 μg purified recombinant IMPDH1 to buffer in 1 cm cuvettes. The initial rate of activity was measured in a temperature-controlled Cary 50 UV–vis spectrophotometer by monitoring the absorbance increase at 340 nm for 1 min owing to the formation of reduced NAD (NADH) from NAD+, and Cary WinUV software was used to measure reaction rates.

Expression of wild-type and mutant His-tagged IMPDH1 in HEK 293T cells

The wild-type and mutant *IMPDH1* cDNA sequences were sub-cloned from the pET15b vector by cutting with *Xho*I, inserts were blunt-ended and ligated into the blunted *Acc651* site of the pcDNA3.1/HisC vector (Invitrogen), which incorporates an N-terminus His-tag in the resulting protein. Human embryonic kidney 293 (HEK 293T) cells were cultured in DMEM with 10% fetal bovine serum at 37°C and an atmosphere of 5% CO_2. Cells were seeded at a density of 10^6 cells per 10 cm dish overnight and were transiently transfected using 20 μg of DNA and the calcium phosphate method. Cells were harvested by trypsinization after 48 h, washed twice with PBS and centrifuged gently to pellet. A protein isolation protocol for extraction of cell fractions was adapted from Deery *et al.* (29). Cell pellet from one dish of cells was resuspended in 1 ml buffer A (10 mM HEPES pH 7.9, 1.5 mM $MgCl_2$, 10 mM KCl, 0.5 mM DTT, 0.5 mM PMSF, 0.25 mM benzamidine). Cells were incubated on ice for 10 min then re-pelleted by spinning for 10 min in a microfuge at 2000 rpm at 4°C. Cells were resuspended in 300 μl buffer A, and for each prep a 100 μl sample was removed for whole cell protein analysis. NaCl was added to this aliquot to a concentration of 1 M to lyse all membranes. To the remaining 200 μl of cell suspension detergent Nonidet P-40 was added to a concentration of 0.2%, the mixture was incubated on ice for 10 min and the suspension was spun at 3500 rpm for 10 min at 4°C. The supernatant which contains the soluble cytosolic proteins was removed. The pellet containing nuclei and insoluble components was resuspended in 200 μl buffer B (5 mM HEPES pH 7.9, 1.5 mM $MgCl_2$, 0.2 mM EDTA, 0.5 mM PMSF, 0.25 mM benzamidine) and NaCl was added to a final concentration of 1 M. After 45 min incubation at 4°C, nuclear lysis occurs and viscosity was reduced by shearing DNA and passing 10 times through a 25 gauge needle. The suspension was then spun at 13000 rpm for 40 min at 4°C. The supernatant containing soluble nuclear proteins was preserved. The final pellet was resuspended in 100 μl of 1% SDS to denature and solubilize remaining proteins. Protein concentrations were then measured using BioRad Protein assay kit with bovine IgG as standard.

SDS–PAGE and western analysis of protein extracts

Aliquots containing equal amounts of total protein (30 μg) were loaded onto 10% SDS–PAGE gels in duplicate. One gel was stained with Coomassie blue and the proteins on the second gel were transferred by electroblotting onto nitrocellulose membrane. Blots were blocked with 1% casein in TBS (Novagen) and then probed with an Anti His-tag monoclonal antibody (Novagen 200 ng/ml). After washing, the blots were probed with a horseradish peroxidase-conjugated anti-mouse IgG secondary antibody (Sigma) and signal was detected using SuperSignal West Pico Chemiluminescent Substrate (Pierce) according to the manufacturer's instructions.

Protein modelling computational methods

Homology modelling. The IMPDH-2 crystal structure entries 1B3O (*Homo sapiens*) and 1JR1 (*Cricetulus griseus*) were downloaded from the PDB database (www.rcsb.org). The manually edited structures for chain B of 1B30 and chain A of 1JR1 were read into the InsightII molecular modelling programme. The protein sequences were extracted and superposed using the structure alignment tool in the homology module. Any resultant alignment errors corrected manually. The sequence of the wild-type IMPDH-1 protein was loaded into the homology module. Coordinates were assigned using those residues conserved between the wild-type sequence and 1B3O. Where conservation was not present for wild-type and 1B3O, but possible for 1JR1, the coordinates were assigned using the latter structure. The resultant model had coordinates assigned for 90.1% of the sequence and was saved once null coordinate residues were pruned. The mutant structure was created by replacing Arg 224 with a proline residue in the Biopolymer module of InsightII. Both structures were subjected to the energy minimisation protocol detailed below before initiating molecular dynamics studies.

Energy minimizations. For all crystals, hydrogens were added assuming a pH of 7.4 and standard amino acid pK_a values using the Biopolymer module in Insight 2000 (Accelrys). The CFF forcefield was used throughout all the minimizations and subsequent MD simulations. No cut-offs were used to treat non-bonded interactions, while a fixed dielectric constant of 4.0 was used for computing electrostatic interactions. The protein structure was subjected to an energy minimization, using the Discover 3 module in Insight 2000 (Accelrys). This initial energy minimization was carried out in a staged manner to prevent strong steric clashes from perturbing greatly the initial conformation. Van der Waals interactions were scaled down to 33% of their real value and a minimization of 100 steps using steepest descents was performed. Van der Waals

interactions were then scaled up to 66% of their real value and a second minimization of 100 steepest descents steps was carried out. Van der Waals interactions were then scaled up to 100% of their real value and a third and final minimization of 250 steepest descents steps was then conducted. Following this a conjugate-gradient minimization of 500 steps was executed.

Molecular dynamics. A series of molecular dynamics (MD) simulations were carried out on the JR1 wild-type and mutant X-ray structures as well as on the homology model wild-type and mutant structures in order to efficiently explore conformational space. All MD simulations were conducted using the Discover 3 module in Insight 2000 (Accelrys) and the following conditions were applied. A canonical (N, V, T) ensemble was used and the Nosé–Hoover thermostat (44) was applied to keep the temperature at 300 K. The Verlet velocity method (45) was employed to integrate the equations of motion, with a timestep of 0.5 fs, and the RATTLE algorithm was applied to constrain all bonds. The initial velocities were assigned randomly to match a Boltzmann distribution of the temperature. An initial equilibration period of 10 000 steps (5 ps) was allowed before proceeding to collection periods of 1 000 000 steps (500 ps) in each MD simulation. No other constraints were applied to the simulations and the whole protein structure was allowed to have full conformational flexibility. After the MD simulations were completed, the stored configurations were subjected to full energy minimizations. Initially, 500 steps of steepest descents were carried out, followed by a second minimization stage using conjugate gradients with the Fletcher-Reeves method (46) up to a convergence gradient of 0.01 kcal mol^{-1} $Å^{-1}$.

URLs

The Unigene database is available at www.ncbi.nlm.nih.gov/entrez/query.fcgi?db = unigene. The retinal information network RetNet is available at www.sph.uth.tmc.edu/Retnet/. Retina International's database can be found at www.retina-international.org/sci-news/database.htm/.

ACKNOWLEDGEMENTS

The authors would especially like to thank Dr Steve Daiger and Dr Sara Bowne, University of Texas, Houston, for helpful and ongoing discussion. This work has been supported by grants from the Wellcome Trust, the Health Research Board of Ireland, Science Foundation Ireland, the British RP Society, the Foundation Fighting Blindness (USA), Fighting Blindness Ireland, and the European Union 5th Framework Programme (HPRN-CT-2000-00098; QLK6-CT-2001-00385). The Ocular Genetics Unit is a member of the HEA-Ireland-sponsored Biopharmaceutical Science Network.

REFERENCES

1. Heckenlively, J.R. (1988) Retinitis pigmentosa. In Heckenlively, J.R. (ed.), *Retinitis Pigmentosa*. J.B. Lippincott, Philadelphia, PA, pp. 1–5.
2. Weleber, R.G. and Gregory-Evans, K. (2001) Retinitis pigmentosa and allied disorders. In Ryan, S.J. (ed.), *Retina*. Mosby, St Louis, MO, pp. 362–470.
3. Rivolta, C., Sharon, D., DeAngelis, M.M. and Dryja, T.P. (2002) Retinitis pigmentosa and allied diseases: numerous diseases, genes, and inheritance patterns. *Hum. Mol. Genet.*, **11**, 1219–1227.
4. Farrar, G.J., Kenna, P.F. and Humphries, P. (2002) On the genetics of retinitis pigmentosa and on mutation-independent approaches to therapeutic intervention. *EMBO J.*, **21**, 857–864.
5. Mansergh, F.C., Millington-Ward, S., Kennan, A., Kiang, A.S., Humphries, M., Farrar, G.J., Humphries, P. and Kenna, P.F. (1999) Retinitis pigmentosa and progressive sensorineural hearing loss caused by a C12258A mutation in the mitochondrial MTTS2 gene. *Am. J. Hum. Genet.*, **64**, 971–985.
6. Vithana, E.N., Abu-Safieh, L., Allen, M.J., Carey, A., Papaioannou, M., Chakarova, C., Al-Maghtheh, M., Ebenezer, N.D., Willis, C., Moore, A.T. *et al.* (2001) A human homolog of yeast pre-mRNA splicing gene, PRP31, underlies autosomal dominant retinitis pigmentosa on chromosome 19q13.4 (RP11). *Mol. Cell*, **8**, 375–381.
7. Chakarova, C.F., Hims, M.M., Bolz, H., Abu-Safieh, L., Patel, R.J., Papaioannou, M.G., Inglehearn, C.F., Keen, T.J., Willis, C., Moore, A.T. *et al.* (2002) Mutations in HPRP3, a third member of pre-mRNA splicing factor genes, implicated in autosomal dominant retinitis pigmentosa. *Hum. Mol. Genet.*, **11**, 87–92.
8. McKie, A.B., McHale, J.C., Keen, T.J., Tarttelin, E.E., Goliath, R., van Lith-Verhoeven, J.J., Greenberg, J., Ramesar, R.S., Hoyng, C.B., Cremers, F.P. *et al.* (2001) Mutations in the pre-mRNA splicing factor gene PRPC8 in autosomal dominant retinitis pigmentosa (RP13). *Hum. Mol. Genet.*, **10**, 1555–1562.
9. Kennan, A., Aherne, A., Palfi, A., Humphries, M., McKee, A., Stitt, A., Simpson, D.A., Demtroder, K., Orntoft, T., Ayuso, C. *et al.* (2002) Identification of an IMPDH1 mutation in autosomal dominant retinitis pigmentosa (RP10) revealed following comparative microarray analysis of transcripts derived from retinas of wild-type and Rho(−/−) mice. *Hum. Mol. Genet.*, **11**, 547–557.
10. Bowne, S.J., Sullivan, L.S., Blanton, S.H., Cepko, C.L., Blackshaw, S., Birch, D.G., Hughbanks-Wheaton, D., Heckenlively, J.R. and Daiger, S.P. (2002) Mutations in the inosine monophosphate dehydrogenase 1 gene (IMPDH1) cause the RP10 form of autosomal dominant retinitis pigmentosa. *Hum. Mol. Genet.*, **11**, 559–568.
11. Jordan, S.A., Farrar, G.J., Kenna, P., Humphries, M.M., Sheils, D.M., Kumar-Singh, R., Sharp, E.M., Soriano, N., Ayuso, C., Benitez, J. *et al.* (1993) Localization of an autosomal dominant retinitis pigmentosa gene to chromosome 7q. *Nat. Genet.*, **4**, 54–58.
12. Natsumeda, Y., Ohno, S., Kawasaki, H., Konno, Y., Weber, G. and Suzuki, K. (1990) Two distinct cDNAs for human IMP dehydrogenase. *J. Biol. Chem.*, **265**, 5292–5295.
13. Senda, M. and Natsumeda, Y. (1994) Tissue-differential expression of two distinct genes for human IMP dehydrogenase (E.C.1.1.1.205). *Life Sci.*, **54**, 1917–1926.
14. Gu, J.J., Tolin, A.K., Jain, J., Huang, H., Santiago, L. and Mitchell, B.S. (2003) Targeted disruption of the inosine 5′-monophosphate dehydrogenase type I gene in mice. *Mol. Cell. Biol.*, **23**, 6702–6712.
15. Gu, J.J., Stegmann, S., Gathy, K., Murray, R., Laliberte, J., Ayscue, L. and Mitchell, B.S. (2000) Inhibition of T lymphocyte activation in mice heterozygous for loss of the IMPDH II gene. *J. Clin. Invest.*, **106**, 599–606.
16. La Cour, M. (2002) The retinal pigment epithelium. In Kaufman, P.L., Alm, A. (eds), *Adler's Physiology of the Eye*, 10th edn. Mosby, St Louis, MO, pp. 348–357.
17. Colby, T.D., Vanderveen, K., Strickler, M.D., Markham, G.D. and Goldstein, B.M. (1999) Crystal structure of human type II inosine monophosphate dehydrogenase: implications for ligand binding and drug design. *Proc. Natl Acad. Sci. USA*, **96**, 3531–3536.
18. Sintchak, M.D., Fleming, M.A., Futer, O., Raybuck, S.A., Chambers, S.P., Caron, P.R., Murcko, M.A. and Wilson, K.P. (1996) Structure and mechanism of inosine monophosphate dehydrogenase in complex with the immunosuppressant mycophenolic acid. *Cell*, **85**, 921–930.
19. Sintchak, M.D. and Nimmesgern, E. (2000) The structure of inosine 5′-monophosphate dehydrogenase and the design of novel inhibitors. *Immunopharmacology*, **47**, 163–184.
20. Carr, S.F., Papp, E., Wu, J.C. and Natsumeda, Y. (1993) Characterization of human type I and type II IMP dehydrogenases. *J. Biol. Chem.*, **268**, 27286–27290.
21. Hager, P.W., Collart, F.R., Huberman, E. and Mitchell, B.S. (1995) Recombinant human inosine monophosphate dehydrogenase type I and type II proteins. Purification and characterization of inhibitor binding. *Biochem. Pharmac.*, **49**, 1323–1329.

22. Chang, D.K., Cheng, S.F., Trivedi, V.D. and Lin, K.L. (1999) Proline affects oligomerization of a coiled coil by inducing a kink in a long helix. *J. Struct. Biol.*, **128**, 270–279.
23. Flohil, J.A., Vriend, G. and Berendsen, H.J. (2002) Completion and refinement of 3-D homology models with restricted molecular dynamics: application to targets 47, 58, and 111 in the CASP modeling competition and posterior analysis. *Proteins*, **48**, 593–604.
24. Daiger, S.P., Sullivan, L.S., Bowne, S.J., Kennan, A., Humphries, P., Birch, D.G., Heckenlively, J.R. and the RP1 consortium. (2003) Identification of the RP1 and RP10 (IMPDH1) genes causing autosomal dominant RP. In LaVail, M.M., Hollyfield, J.G. and Anderson, R.E. (eds), *Retinal Degenerations*. Kluwer Academic, New York, pp. 1–12.
25. Humphries, M.M., Rancourt, D., Farrar, G.J., Kenna, P., Hazel, M., Bush, R.A., Sieving, P.A., Sheils, D.M., McNally, N., Creighton, P. *et al.* (1997) Retinopathy induced in mice by targeted disruption of the rhodopsin gene. *Nat. Genet.*, **15**, 216–219.
26. Sanyal, S., De Ruiter, A. and Hawkins, R.K. (1980) Development and degeneration of retina in rds mutant mice: light microscopy. *J. Comp. Neurol.*, **194**, 193–207.
27. Gao, J., Cheon, K., Nusinowitz, S., Liu, Q., Bei, D., Atkins, K., Azimi, A., Daiger, S.P., Farber, D.B., Heckenlively, J.R. *et al.* (2002) Progressive photoreceptor degeneration, outer segment dysplasia, and rhodopsin mislocalization in mice with targeted disruption of the retinitis pigmentosa-1 (Rp1) gene. *Proc. Natl Acad. Sci. USA*, **99**, 5698–5703.
28. Furukawa, T., Morrow, E.M., Li, T., Davis, F.C. and Cepko, C.L. (1999) Retinopathy and attenuated circadian entrainment in Crx-deficient mice. *Nat. Genet.*, **23**, 466–470.
29. Deery, E.C., Vithana, E.N., Newbold, R.J., Gallon, V.A., Bhattacharya, S.S., Warren, M.J., Hunt, D.M. and Wilkie, S.E. (2002) Disease mechanism for retinitis pigmentosa (RP11) caused by mutations in the splicing factor gene PRPF31. *Hum. Mol. Genet.*, **11**, 3209–3219.
30. Liu, X., Garriga, P. and Khorana, H.G. (1996) Structure and function in rhodopsin: correct folding and misfolding in two point mutants in the intradiscal domain of rhodopsin identified in retinitis pigmentosa. *Proc. Natl Acad. Sci. USA*, **93**, 4554–4559.
31. Saliba, R.S., Munro, P.M., Luthert, P.J. and Cheetham, M.E. (2002) The cellular fate of mutant rhodopsin: quality control, degradation and aggresome formation. *J. Cell Sci.*, **115**, 2907–2918.
32. Illing, M.E., Rajan, R.S., Bence, N.F. and Kopito, R.R. (2002) A rhodopsin mutant linked to autosomal dominant retinitis pigmentosa is prone to aggregate and interacts with the ubiquitin proteasome system. *J. Biol. Chem.*, **277**, 34150–34160.
33. Sherman, M.Y. and Goldberg, A.L. (2001) Cellular defenses against unfolded proteins: a cell biologist thinks about neurodegenerative diseases. *Neuron*, **29**, 15–32.
34. Kopito, R.R. (2000) Aggresomes, inclusion bodies and protein aggregation. *Trends Cell. Biol.*, **10**, 524–530.
35. Bence, N.F., Sampat, R.M. and Kopito, R.R. (2001) Impairment of the ubiquitin-proteasome system by protein aggregation. *Science*, **292**, 1552–1555.
36. Acland, G.M., Aguirre, G.D., Ray, J., Zhang, Q., Aleman, T.S., Cideciyan, A.V., Pearce-Kelling, S.E., Anand, V., Zeng, Y., Maguire, A.M. *et al.* (2001) Gene therapy restores vision in a canine model of childhood blindness. *Nat. Genet.*, **28**, 92–95.
37. Smith, A.J., Schlichtenbrede, F.C., Tschernutter, M., Bainbridge, J.W., Thrasher, A.J. and Ali, R.R. (2003) AAV-Mediated gene transfer slows photoreceptor loss in the RCS rat model of retinitis pigmentosa. *Mol. Ther.*, **8**, 188–195.
38. Bowne, S.J., Gire, A., Sullivan, L.S., Heckenlively, J.R., Birch, D.G., Hughbanks-Wheaton, D., Lewis, R.A. and Daiger, S.P. (2003) Frequency and spectrum of IMPDH1 mutations associated with autosomal dominant retinitis pigmentosa. *Invest. Ophthal. Visual Sci.*, **44**, E-Abstract 2307.
39. Millington-Ward, S., O'Neill, B., Tuohy, G., Al-Jandal, N., Kiang, A.S., Kenna, P.F., Palfi, A., Hayden, P., Mansergh, F., Kennan, A., Humphries, P. and Farrar, G.J. (1997) Strategems *in vitro* for gene therapies directed to dominant mutations. *Hum. Mol. Genet.*, **6**, 1415–1426.
40. Millington-Ward, S., O'Neill, B., Kiang, A.S., Humphries, P., Kenna, P.F. and Farrar, G.J. (1999) A mutation-independent therapeutic strategem for osteogenesis imperfecta. *Antisense Nucl. Acid Drug. Dev.*, **9**, 537–542.
41. O'Neill, B., Millington-Ward, S., O'Reilly, M., Tuohy, G., Kiang, A.S., Kenna, P.F., Humphries, P. and Farrar, G.J. (2000) Ribozyme-based therapeutic approaches for autosomal dominant retinitis pigmentosa. *Invest. Ophthal. Visual Sci.*, **41**, 2863–2869.
42. McManus, M.T. and Sharp, P.A. (2002) Gene silencing in mammals by small interfering RNAs. *Nat. Rev. Genet.*, **3**, 737–747.
43. Miller, V.M., Xia, H., Marrs, G.L., Gouvion, C.M., Lee, G., Davidson, B.L. and Paulson, H.L. (2003) Allele-specific silencing of dominant disease genes. *Proc. Natl Acad. Sci. USA*, **100**, 7195–7200.
44. Nosé, S. (1991) Constant temperature molecular-dynamics methods. *Prog. Theor. Phys. Suppl.*, **103**, 1–46.
45. Swope, W.C., Andersen, H.C., Berens, P.H. and Wilson, K.R. (1982) A computer simulation method for the calculation of equilibrium constants for the formation of physical clusters of molecules: application to small water clusters. *J. Chem. Phys.*, **76**, 637–649.
46. Fletcher, R. (1980). *Practical Methods of Optimization, Vol. 1. Unconstrained Optimization*. Wiley, New York.